JOURNAL OF MATERIALS SCIENCE 27 (1991) 3143–3154

Interfacial debonding and fibre pull-out stresses

Part I *Critical comparison of existing theories with experiments*

JANG-KYO KIM, C. BAILLIE, YIU-WING MAI
Centre for Advanced Materials Technology, Department of Mechanical Engineering, University of Sydney, Sydney, NSW 2006, Australia

Two current theories [11, 17] of interfacial debonding and fibre pull-out, which have been developed on the basis of fracture mechanics and shear strength criteria, respectively, are critically compared with experimental results of several composite systems. From the plots of partial debond stress, σ_d^p, as a function of debond length, three different cases of the interfacial debond process can be identified, i.e. totally unstable, partially stable and totally stable. The stability of the debond process is governed not only by elastic constants, relative volume of fibre and matrix but more importantly by the nature of bonding at the interface and embedded fibre length, L. It is found that for the epoxy-based matrix composite systems, Gao *et al.*'s model [17] predicts the trend of maximum debond stress, σ_d^*, very well for long L, but it always overestimates σ_d^* for very short L. In contrast, Hsueh's model [11] has the capability to predict σ_d^* for short L, but it often needs significant adjustment to the bond shear strength for a better fit of the experimental results for long L. For a ceramic-based matrix composite, σ_d^* predicted by the two models agree exceptionally well with experiment over almost the whole range of L, a reflection that the assumed stable debond process in theory is actually achieved in practice. With respect to the initial frictional pull-out stress, σ_f, the agreement between the two theories and experiments is excellent for all range of L and all composite systems, suggesting that the solutions for σ_f proposed by the two models are essentially identical. Although Gao *et al.*'s model has the advantage to determine accurately the important interfacial properties such as residual clamping stress, q_0, and coefficient of friction, μ, it needs some modifications if accurate predictions of σ_d^* are sought for very short L. These include varying interfacial fracture toughness, G_{ic} with debond crack growth, unstable debonding for very short L and inclusion of shear deformation in the matrix for the evaluation of G_{ic} and fibre stress distribution. Hsueh's model may also be improved to obtain a better solution by including the effect of matrix axial stress existing at the debonded region on the frictionless debond stress, σ_0.

1. Introduction

As the use of advanced fibre composite materials in engineering application is extended, fundamental considerations of cost and structural efficiency are augmented by improving design reliability. This requires a basic understanding of how the fracture process initiates and progresses to final failure. Of particular importance during fracture is the local response of the fibre–matrix interface which has pronounced effects on the mechanical performance and structural integrity of the composite. Experience has shown that when a crack moves through a matrix containing fibres, energies are absorbed by the failure mechanisms such as matrix cracking, fibre–matrix interfacial debonding, post-debonding friction, fibre fracture, stress redistribution, fibre pull-out, etc., among which debonding and frictional sliding during fibre pull-out provide major contributions to the fracture toughness of most fibre composites with polymer- and ceramic-based matrices. Therefore, optimal conditions for toughening of fibre composites require these mechanisms to occur properly, which in turn needs proper control of the interfacial properties. A comprehensive review on how the interfacial properties influence the strength and fracture toughness of fibre composites, including the various methods for improving the fracture toughness by means of interface control, was recently given by Kim and Mai [1].

Several experimental techniques have been developed to characterize the interfacial properties including the single fibre pull-out test [2], the single fibre fragment test [3], the microdebond test [4] and the fibre push-out (or indentation) test [5]. Among these methods, the most popular and reliable method seems to be the single fibre pull-out test which is the subject of the present study. Theoretical analyses of

0022–2461

the debonding and fibre pull-out problem can be classified into two distinct approaches: one is based on a maximum shear stress criterion such that when the interfacial shear stress exceeds the shear bond strength, complete debonding occurs unstably; and the other is based on the concept of fracture mechanics where the debonded zone is considered as an interfacial crack and its extension is dependent on the energy criterion being satisfied. The first approach is typified by the early work of Cox [6], Greszczuk [7] and Takaku and Arridge [8] based on the "shear lag" model, namely that the tensile stresses in the matrix are negligible relative to those in the fibres, whereas the shear stresses in the fibres are small compared to those in the matrix. Lawrence and co-workers [9, 10] have included the effect of frictional shear stress opposing the pull-out at the debonded region. The shear strength criterion has been modified recently in a series of studies by Hsueh [11, 12] who postulated that a progressive stable debonding exists along the interface and considered the effect of shear deformation in the matrix. Representative work of the fracture mechanics approach includes those of Gurney and Hunt [13], Outwater and Murphy [14] and Stang and Shah [15]. Following the argument of previous workers [15, 16] that the fracture mechanics approach to the debonding problem is preferred to the maximum shear stress criterion, Gao *et al.* [17] have presented a rigorous analysis where a pre-debonded interface is modelled as a crack propagating stably along the interface with a constant interfacial fracture toughness (or specific energy absorption) under plane strain condition. Both the effects of friction at the debonded region and Poisson contraction of the fibre are included in the Hsueh [11, 12] and Gao *et al.* [17] analyses. All these above studies assume zero interface thickness and uniform homogeneous matrix properties so that any difference in properties of the matrix material immediately surrounding the fibre (i.e. commonly referred to as the "interphase" as contrast to the bulk matrix material) is neglected.

The principal aim of the present study is to enhance our understanding of the debonding and fibre pull-out problem by (i) identifying the similarities and differences between the two debond criteria mentioned above, (ii) evaluating critically the validity and discrepancy of the assumptions made in each criterion, and (iii) providing possible solutions for improved theories. For this purpose, two typical models, i.e. Gao *et al.* [17] and Hsueh [11, 12], representing the fracture mechanics- and shear strength-based criteria, respectively, are used to compare with experimental results of several different composite systems.

2. Current theories for fibre debond and pull-out

Both Gao *et al.* [17] and Hsueh [11, 12] considered a shear lag model where a fibre (with radius a) is located at the centre of a coaxial cylindrical shell of matrix (with an outer radius b) as shown in Fig. 1. z is the direction parallel to the fibre axis and L is the total embedded fibre length. In the fibre pull-out experiments, the composite is fixed at one end ($z = 0$) and a tensile stress is applied at the other end ($z = L$) of the embedded fibre with a constant displacement or loading rate. Both models assume that the debond crack propagates from the loaded end of the fibre so that any effect arising from considering debond crack propagation from the embedded fibre end ($z = 0$), the so-called "two-way debonding" [18–20], is neglected.

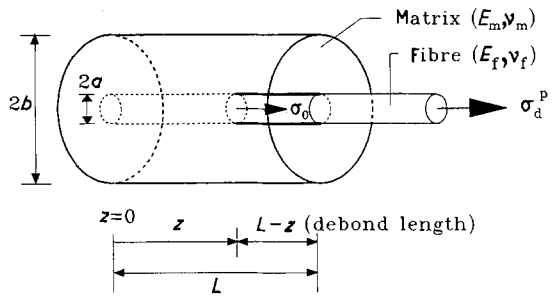

Figure 1 A schematic drawing of the partially debonded fibre in a fibre pull-out model.

2.1. The Gao–Mai–Cotterell model

Gao *et al.*'s model [17] assumes a pre-debonded region ($L - z$) as a pre-crack in the context of fracture mechanics, deriving the partial debond stress, σ_d^p, as a function of the partial debond length ($L - z$)

$$\sigma_d^p = \sigma_0 + (\bar{\sigma} - \sigma_0)\left\{\frac{\exp[\lambda(L - z)] - 1}{\exp[\lambda(L - z)] - 1 + \theta}\right\} \approx \sigma_0 + (\bar{\sigma} - \sigma_0)\{1 - \exp[-\lambda(L - z)]\} \quad (1a)$$

where

$$\theta = \frac{1 + (\gamma/\alpha)(\nu_m/\nu_f)}{1 + (\gamma/\alpha)[(1 - 2k\nu_m)/(1 - 2k\nu_f)]} \approx 1 \quad \text{for } b^2 \gg a^2 \quad (1b)$$

where σ_0 is the frictionless debond stress independent of z, λ is the reciprocal length giving the effective shear stress transfer distance and $\bar{\sigma}$ is the asymptotic debond stress for long embedded length, L. The experimentally determined parameters σ_0, λ and $\bar{\sigma}$ are related to the interfacial fracture toughness, G_{ic}, the coefficient of friction at the interface, μ, and the residual clamping stress, q_0, by

$$\sigma_0 = \left\{\frac{4E_fG_{ic}[(1 - 2k\nu_f) + (\gamma/\alpha)(1 - 2k\nu_m)]}{a(1 - 2k\nu_f)^2}\right\}^{1/2} \approx \left[\frac{4E_fG_{ic}}{a(1 - 2k\nu_f)}\right]^{1/2} \quad (2a)$$

$$\lambda = 2\mu k/a \quad (2b)$$

$$\bar{\sigma} = -(q_0/k)[1 + (\gamma/\alpha)(\nu_m/\nu_f)] \quad (2c)$$

where $\alpha = E_m/E_f$ (Young's modulus ratio of the matrix to the fibre), $\gamma = a^2/(b^2 - a^2)$ (fibre volume fraction) and $k = (\alpha\nu_f + \gamma\nu_m)/[\alpha(1 - \nu_f) + 1 + \nu_m + 2\gamma]$. ν_f and ν_m are the fibre and matrix Poisson ratios. The solution for the initial frictional pull-out stress, σ_f, after complete debonding can be obtained by substituting $\sigma_0 = 0$ and the partial debond length

$(L - z)$ by the full debond length L (i.e. $z = 0$) in Equation 1a

$$\sigma_f = \bar{\sigma}\left[\frac{\exp(\lambda L) - 1}{\exp(\lambda L) - 1 + \theta}\right] \approx \bar{\sigma}[1 - \exp(-\lambda L)] \quad (3)$$

2.2. The Hsueh model

In Hsueh's model [12], the solution for the partial debond stress, σ_d^p, is given by

$$\sigma_d^p = \sigma_0 + (\bar{\sigma} - \sigma_0) \times \left\{1 - \frac{B_1[1 + (\gamma/\alpha)(\nu_m/\nu_f)]}{\lambda + B_1(\gamma/\alpha)(\nu_m/\nu_f) + B_2}\right\} \approx \sigma_0 + (\bar{\sigma} - \sigma_0)[1 - B_1/(\lambda + B_2)] \quad b^2 \gg a^2 \quad (4)$$

In Equation 4, the frictionless debond stress, σ_0, for the full embedded length, L, is determined from the analytical solution for the fibre stress at the free matrix surface [21] when the interfacial shear stress exceeds the shear bond strength, τ_b

$$\sigma_0 = \{2\tau_b[1 + (\gamma/\alpha)]/\beta a\}\tanh(\beta L) \quad (5a)$$

where

$$\beta = \left\{\frac{1 + (\alpha/\gamma)}{(1 + \nu_m)[b^2\ln(b/a) - (a^2/2\gamma)]}\right\}^{1/2} \quad (5b)$$

The instantaneous σ_0 values during progressive debonding can be determined by replacing L with the bond length z. It should be noted that for $b^2 \gg a^2$, as in usual fibre pull-out experiments, Equation 5a is simplified to $\sigma_0 = [2\tau_b/\beta a]\tanh(\beta L)$, which is the same solution for maximum debond stress, σ_d^*, given in earlier papers [6–8], when there is no friction at the debonded region. The parameters B_1 and B_2 are a function of partial debond length $(L - z)$

$$B_1 = \frac{(m_1 - m_2)\exp[(m_1 + m_2)(L - z)]}{\exp[m_1(L - z)] - \exp[m_2(L - z)]} \quad (6a)$$

$$B_2 = \frac{m_1\exp[m_1(L - z)] - m_2\exp[m_2(L - z)]}{\exp[m_1(L - z)] - \exp[m_2(L - z)]} \quad (6b)$$

where $m_1 = -[\Omega + (\Omega^2 - 4\Omega\lambda)^{1/2}]/2$ and $m_2 = -[\Omega - (\Omega^2 - 4\Omega\lambda)^{1/2}]/2$. $\Omega = -(\beta^2/\lambda)\{[1 + (\alpha/\gamma)(\nu_f/\nu_m)]/[1 + (\alpha/\gamma)]\}$, which can be simplified to $\Omega \approx -(\beta^2/\lambda)(\nu_f/\nu_m)$ for $b^2 \gg a^2$. The solution for the initial frictional pull-out stress, σ_f, is obtained by substituting $\sigma_0 = 0$ in Equation 4 in a way similar to Equation 3 as

$$\sigma_f = \bar{\sigma}\left\{1 - \frac{B_1[1 + (\gamma/\alpha)(\nu_m/\nu_f)]}{\lambda + B_1(\gamma/\alpha)(\nu_m/\nu_f) + B_2}\right\} \approx \bar{\sigma}[1 - B_1/(\lambda + B_2)] \quad \text{for } b^2 \gg a^2 \quad (7)$$

In Equation 7, the parameters B_1 and B_2 are determined from Equation 6 with $z = 0$.

The two theories discussed above are similar in that σ_d^p is composed of two components: a frictionless debond stress component and a friction stress component. The second component is directly proportional to $(\bar{\sigma} - \sigma_0)$ and is also controlled by λ (or the coefficient of friction, μ). However, there is an obvious difference in the first component regarding the frictionless debond stress, σ_0, as can be seen in Equations 2a and 5a. In Gao *et al.*'s model, σ_0 is invariant with the embedded fibre length, L, and it depends only on the interfacial fracture energy, G_{ic}. In contrast, in Hsueh's model, σ_0 is a function of bond length, z, and it approaches a constant value for long z as $\tanh \beta z$ becomes unity. Instead of G_{ic} the frictionless debond stress, σ_0, is now controlled by the shear bond strength, τ_b.

3. Comparison between theories and experiments

3.1. Single-fibre pull-out tests

Single-fibre pull-out tests were performed on composite systems of (both untreated and electrolytically oxidized) carbon fibres (XAU) embedded in an epoxy matrix (a DGEBA, Araldite MY 750 with hardener HY 951 in the ratio of 100:12 by weight) with elastic constants and radii given by $E_f = 230$ GPa, $E_m = 3.0$ GPa, $\nu_f = 0.2$, $\nu_m = 0.4$, $a = 0.003$ mm and $b = 1.0$ mm. Tests were also performed on model composites of (both uncoated and release-agent coated) stainless steel wire–epoxy matrix (a DGEBA, Araldite GY 260 with curing agent piperidine in the ratio of 100:5 by weight) for which $E_f = 179$ GPa, $E_m = 3.0$ GPa, $\nu_f = 0.3$, $\nu_m = 0.35$, $a = 0.275$ mm and $b = 6.5$ mm. Fibres were pulled from the matrix using an Instron testing machine with cross-head speed 0.05 and 0.5 mm min^{-1}, respectively, for the carbon fibre– and steel wire–epoxy matrix composite systems. The pull-out force–displacement curves were obtained and used to determine the maximum debond stress σ_d^* and the initial frictional pull-out stress, σ_f, based on the force values at the points just before and after the instantaneous load drop. The frictionless initial debond stress, σ_0, for Gao *et al.*'s model is also recorded when an instantaneous small load drop was first observed in the rising stress–displacement record, as suggested previously [17]. For the carbon fibre–epoxy matrix composite system the embedded fibre length, L, was measured after the pull-out test using a scanning electron microscope.

In an effort to provide more general comparisons, published data for a composite system of SiC fibres embedded in a borosilicate glass matrix [22] ($E_f = 400$ GPa, $E_m = 70$ GPa, $\nu_f = 0.17$, $\nu_m = 0.2$, $a = 0.071$ mm and $b = 2.8$ mm) were also analysed.

3.2. Evaluation of interfacial parameters σ_0, λ and $\bar{\sigma}$

To calculate the predicted values for the maximum debond stress, σ_d^*, and the frictional pull-out stress, σ_f, it is necessary to determine the parameters σ_0, λ and $\bar{\sigma}$ which are functions of the material properties, G_{ic} (or τ_b), μ and q_0, respectively. These properties are seldom measured accurately and reported values for a similar composite system (even if available) cannot be

TABLE I Fibre pull-out parameters and interfacial properties for different fibre composites

Composite system	Fibre surface condition	Fibre pull-out parameters				Interfacial properties				
		σ_0[a] (GPa)	λ (mm^{-1})	$\bar{\sigma}$ (GPa)	z_{max} (mm)	G_{ic}[a] ($J\,m^{-2}$)	μ	q_0 (MPa)	τ_b[b] (MPa)	τ_f (MPa)
Carbon fibre–epoxy matrix	Both untreated and oxidized	3.4	1.5	5.4	0.152	37.7	1.25	− 9.97	72.7	12.2
Steel wire–epoxy matrix	Uncoated	1.95	0.0142	2.41	7.8	1316	0.48	− 8.85	43.5	5.0
	Release-agent coated	0.316	0.0065	1.98	6.5	34.7	0.22	− 7.28	8.96	1.77
SiC fibre–glass matrix	Untreated	0.149	0.0304	2.92	0.06	0.964	0.048	− 64.5	3.18	3.11
	Acid treated	0.235	0.049	3.27	0.08	2.40	0.078	− 72.3	5.83	5.60

[a] Applies to Gao *et al.*'s model.
[b] Applies to Hsueh's model.

directly applied. This implies that fibre debond theories should provide a systematic means to determine these properties with reasonable accuracy, rather than adjusting them to fit the theoretical predictions to experimental results based on a trial and error method.

In fact, Gao *et al.*'s model has such an advantage to evaluate these parameters. It will be shown later that for Gao *et al.*'s model, the maximum debond stress, σ_d^*, is always obtained at the moment of complete debonding when the debond crack reaches the full embedded length, L, and the initial frictional pull-out stress, σ_f, after complete debonding is also a function of the full debond length, L. Therefore, once the relationships of σ_d^* versus L and σ_f versus L are empirically obtained, the independent parameters σ_0, λ and $\bar{\sigma}$ can be determined on the basis of the solutions for σ_d^* and σ_f. Rearrangement of Equations 3 and 1a which are a function of L gives

$$\lambda = -(1/L)\ln[1 - (\sigma_f/\bar{\sigma})] \quad (8a)$$

$$\sigma_0 = (\sigma_d^* - \sigma_f)\exp(\lambda L) = \bar{\sigma}(\sigma_d^* - \sigma_f)/(\bar{\sigma} - \sigma_f) \quad (8b)$$

If data for the frictionless initial debond stress, σ_0, are available directly from the fibre pull-out tests, λ and $\bar{\sigma}$ are easily determined using a linear least squares analysis of Equations 8a and b. Alternatively, the initial gradient can be taken from the linear region of the experimental σ_f versus L curves which is equal to the derivative of the solution for σ_f in Equation 3 with respect to the full debond length, L

$$(d\sigma_f/dL)_{L=0} = \lambda\bar{\sigma} \quad (8c)$$

In using Equation 8b in conjunction of Equations 8a and c, it is necessary to avoid the experimental σ_d^* data obtained for very short embedded fibre length, L, since Gao *et al.*'s model was developed basically for long L.

A similar treatment cannot be made for Hsueh's model to determine the fibre pull-out parameters. This is because the maximum debond stress, σ_d^*, is a complex function of the bond length z as well as the partial debond length $(L - z)$ for a given embedded fibre length L, to be shown in Section 3.3. However, an average value for the shear bond strength, τ_b, can be determined from the initial gradient taken of the experimental maximum debond stress, σ_d^*, versus L curve as

$$(d\sigma_d^*/dL)_{L=0} = 2\tau_b[1 + (\gamma/\alpha)]/a \quad (8d)$$

The values of the fibre pull-out parameters and the interfacial properties determined based on Equations 8a–d for the different composite systems are given in Table I. It is worth noting that the frictionless initial debond stress, σ_0, value (= 316 MPa) determined by using Equation 8b for the release-agent coated steel wire–epoxy matrix composites is approximately equal to the average value (= 304 ± 102 MPa, as shown in Fig. 2) of those obtained directly from the experiment during stable debonding. However, for the reasons to be described later, only a few observations of such initial debonding were obtained for the other composite systems tested by the authors. It is, therefore, not possible to make similar comparisons. Details on the experimental σ_0 values have not been reported for the SiC fibre–glass matrix composites [22].

3.3. Partial debond stress, σ_d^p, and instability of debond process

In a previous study by the authors [23], three different cases of debond process with regard to instability have

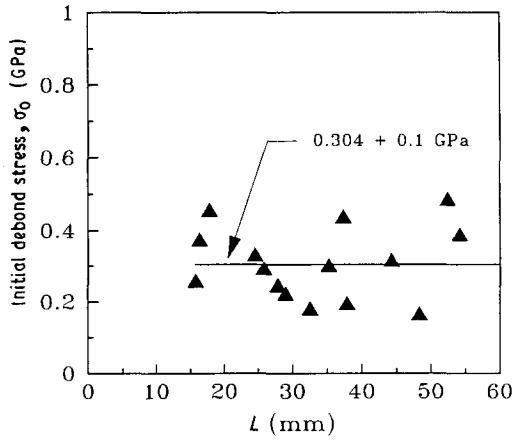

Figure 2 Frictionless initial debond stress, σ_0, values determined from the pull-out test of release-agent coated wire–epoxy matrix composites.

been identified by comparison of the partial debond stress, σ_d^p, which is the sum of the frictionless debond and friction stress components, for different embedded fibre lengths. In the present study, the results for the carbon fibre–epoxy matrix composite are plotted against partial debond length $(L - z)$ (Fig. 3), and its implication on the instability condition of the debond process which, in turn, determines the maximum debond stress, σ_d^*, is discussed in more detail.

For a given L, as debond length $(L - z)$ increases the friction stress component always increases steadily in both theories, the increase being non-linear due to Poisson contraction of the fibre in the debonded region. However, the frictionless debond stress component varies according to the assumptions made in each theory. If a constant σ_0 value is assumed regardless of the embedded fibre length L (i.e. constant G_{ic} in Gao *et al.*'s model [17] and a maximum σ_0 value for long L where $\tanh(\beta z) \approx 1$ in Hsueh's model [11]), the partial debond stress, σ_d^p, increases with the same rate as the friction stress component (Fig. 3a). Therefore, the maximum debond stress, σ_d^*, is obtained always at the moment of complete debonding when the debond crack reaches the full embedded length (i.e. $z = 0$), and consequently the solutions for the maximum debond stress, σ_d^*, in Gao *et al.*'s and Hsueh's models become always a function of the entire embedded length, L, i.e. for Gao *et al.*'s model [11]

$$\sigma_d^* = \sigma_0 + (\bar{\sigma} - \sigma_0)[1 - \exp(-\lambda L)] \quad (9)$$

Indeed, with this assumption, good agreement was reported [11, 17] for the maximum debond stress, σ_d^*, as well as the initial frictional pull-out stress, σ_f, predicted by both theories when compared with the same experimental results obtained by Takaku and Arridge [8] on sufficiently long embedded fibre lengths. In this comparison [11], Hsueh used a constant (i.e. maximum) value for σ_0 independent of L, in contrast to the adoption of a non-constant σ_0 in his later study [12].

However, if it is assumed that the instantaneous σ_0 values vary as a function of bond length z during the fibre debond process as in Hsueh's model [12], the debond stress component decreases toward zero depending on the fibre embedded length, L: for short L, it decreases from the beginning while for long L it is initially constant (i.e. $\tanh(\beta z) = 1$) and decreases to zero (Fig. 3b). Because the friction stress component always increases with $(L - z)$ these two stress components balance each other to determine the instantaneous values of partial debond stress, σ_d^p. This implies that whether σ_d^p decreases from the beginning or increases to a maximum and then decreases during the fibre debond process for a given composite system depends on the embedded fibre length, L. In this case, the maximum debond stress, σ_d^*, is significantly greater than the stress obtained at the moment of complete debonding at $z = 0$ as can be seen in Fig. 3b. In practical fibre pull-out experiments, however, the maximum stress leads immediately to complete debonding followed by a precipitous load drop so that the gradual stress decrease after the maximum as shown in Fig. 3b can never be visualized in the pull-out stress versus displacement curve. For this reason, the maximum debond stress is often incorrectly interpreted as being the same as the complete debond stress.

The instability condition requires that the derivative of the partial debond stress, σ_d^p, with respect to the bond length, z, is equal to or less than zero, i.e. $d\sigma_d^p/dz \leqslant 0$ [23]. In other words, the fibre debond process becomes unstable when the slope of the curve σ_d^p is zero where the maximum debond stress, σ_d^*, is obtained. For an assumed constant frictionless debond stress (Fig. 3a), fibre debonding is always stable until complete debonding at $z = 0$ where $\sigma_d^p = \sigma_d^*$. However, for a varying debond stress component (Fig. 3b), the stability of the debond process is dependent on the partial debond length $(L - z)$ relative to the embedded fibre length, L, and there is a maximum bond length, z_{max}, below which the debond process becomes unstable [9, 10]. The values for z_{max} determined by numerical treatment of Hsueh's theory in Equation 4 with the bond length (z)-dependent frictionless debond stress, σ_0, are given in Table I. It is interesting to note that for the SiC fibre–glass matrix composite, z_{max} values are very small (i.e. $z_{max} \approx 0$) whether the fibres are acid treated or not. If a simplified solution for the partial debond stress proposed

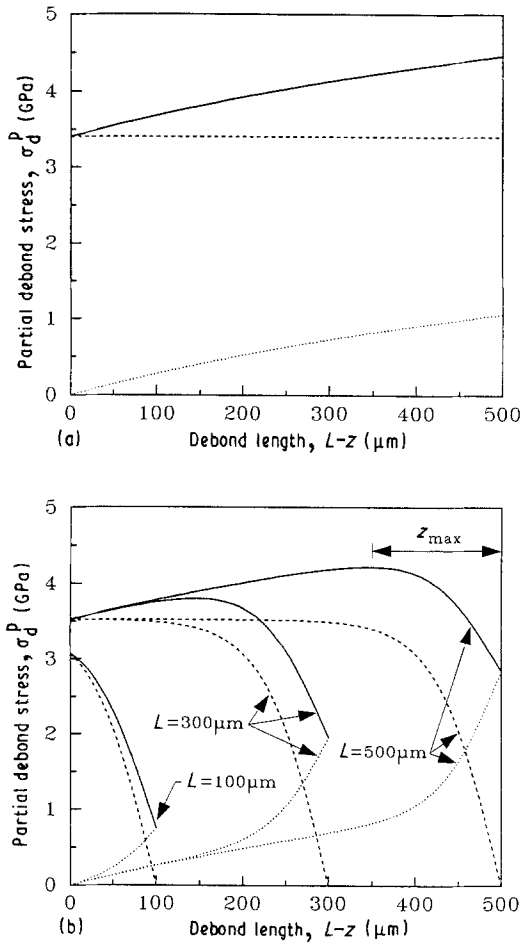

Figure 3 Plots of partial debond stress, σ_d^p, as a function of debond length $(L - z)$ calculated based on (a) Equation 1 of Gao *et al.*'s [17] model and (b) Equation 4 of Hsueh's [12] model for carbon fibre–epoxy matrix composites: (---) frictionless debond stress component; (. . .) friction stress component; (——) partial debond stress.

by Karbhari and Wilkins [24] (i.e. $\sigma_d^p = \sigma_0 + 2\tau_f (L - z)/a$) is used, neglecting the effect of Poisson contraction of the fibre and assuming a constant friction shear stress, τ_f, at the debonded region in the context of the maximum shear strength criterion, the above instability condition gives a closed form solution for the maximum bond length, z_{max} [24]

$$z_{max} = (1/\beta) \cosh^{-1} [(\tau_b/\tau_f)(1 + \gamma/\alpha)]^{1/2} \quad (10)$$

which is basically the same equation given earlier by Lawrence [9]. It is obvious from Equation 10 that the ratio of τ_b to τ_f, Young's modulus ratio, α, fibre volume fraction, γ and β (which is again a function of α and γ), determine the fibre debonding instability for a given composite system, with the limiting value of zero when $\tau_b \approx \tau_f$ (e.g. SiC fibre–glass matrix composites [22], as shown in Table I, where the interfacial bonding is principally mechanical in nature) and $b^2 \gg a^2$. It is noted that the z_{max} values (e.g. 116 μm and 5.8 mm for the carbon fibre- and release-agent-coated steel wire–epoxy matrix composites, respectively) estimated based on Equation 10 are slightly smaller than the values (152 μm and 6.5 mm) obtained by using Hsueh's theory due to the effect of Poisson contraction of the fibre in the debonded region being neglected which therefore overestimates the friction stress component in the simplified solution. The constant τ_f values given in Table I were determined from the initial gradient taken of the experimental σ_f versus L curves for the different composite systems.

Based on the discussions presented above, three different fibre debond processes can be identified in terms of stability and the corresponding pull-out stress versus displacement curves are schematically shown in Fig. 4. If $L \leqslant z_{max}$, the debond process is totally unstable and initial debond leads immediately to complete debonding (i.e. $\sigma_0 = \sigma_d^*$). Therefore, the stress–displacement curve shows a monotonic increase in stress until debonding is initiated, followed by an instantaneous load drop (Fig. 4a). In this case, neither theories proposed by Gao *et al.* [17] and Hsueh [11, 12] can be directly applied to predict the maximum debond stress, σ_d^*. This is because Gao *et al.*'s model is developed basically for very long embedded fibre lengths and in Hsueh's model the friction stress component no longer exists and stable debonding cannot be obtained. Instead, the maximum debond stress, σ_d^*, is simply given by Equation 5a which is based on the assumption of unstable debonding [6–8]. Totally unstable debonding may also occur when the frictional shear stress in the debonded region is negligible so that z_{max} approaches an infinite value as can be envisaged from Equation 10. In this circumstance, Equation 5a also satisfies the solution for the maximum debond stress, σ_d^*. However, when considering the fact that a major toughening mechanism in most advanced fibre composites is related to the frictional resistance at the interface during fibre pull-out, the situation of zero interfacial friction (i.e. either zero residual clamping stress, q_0, or zero coefficient of friction, μ) seems unlikely in practice. If $L > z_{max}$, then the debond crack propagation takes place in a macroscopically stable manner, though "stick–slips" are observed in the rising stress–displacement curve (Fig. 4b). Stable debonding proceeds until the debond length reaches $(L - z_{max})$, followed by unstable debonding (i.e. partially stable). Therefore, the maximum debond stress, σ_d^*, can be determined by replacing z with z_{max} in Equation 4. In the extreme case of $z_{max} \approx 0$ as for some ceramic matrix composites, the debond process is always stable until complete debond takes place regardless of embedded fibre length, L. The rising portion of the debond stress versus displacement curve schematically shown in Fig. 4c is typically linear without "stick–slips" and there is no substantial load drop after complete debonding [25]. This is because the interface is, in principle, frictionally bonded and there is little chemical bonding (i.e. G_{ic} or τ_b is small). Therefore, the linear increase in stress represents primarily the frictional shear stress transfer across the interface without virtual debonding until the frictional resistance over the entire embedded fibre length is overcome. The maximum debond stress, σ_d^*, is then approximately equal to the initial frictional pull-out stress, σ_f, because the frictionless debond stress, σ_0 is negligible (due to small G_{ic} or τ_b) and the friction stress component is a function of the entire embedded length, L. Therefore, for three different debond processes, solutions for the maximum debond stress, σ_d^*, in Hsueh's model can be itemized correctly as

$$\sigma_d^* = \{2\tau_b[1 + (\gamma/\alpha)]/\beta a\}\tanh(\beta L) \qquad L \leqslant z_{max} \quad (11a)$$

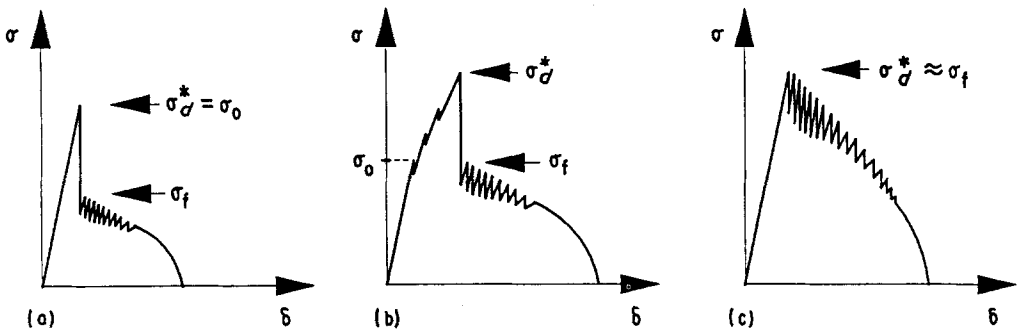

Figure 4 Schematic representation of applied stress, σ, versus displacement, δ, relationship during single-fibre pull-out tests for (a) totally unstable ($L \leqslant z_{max}$) (b) partially stable ($L > z_{max}$) and (c) totally stable ($z_{max} \approx 0$) debond processes.

$$\sigma_d^* = \sigma_0 + (\bar{\sigma} - \sigma_0) \times \left\{1 - \frac{B_1[1 + (\gamma/\alpha)(v_m/v_f)]}{\lambda + B_1(\gamma/\alpha)(v_m/v_f) + B_2}\right\}$$

$$L > z_{max} \quad (11b)$$

$$\sigma_d^* \approx \sigma_f = \bar{\sigma}\left\{1 - \frac{B_1[1 + (\gamma/\alpha)(v_m/v_f)]}{\lambda + B_1(\gamma/\alpha)(v_m/v_f) + B_2}\right\}$$

$$z_{max} \approx 0 \quad (11c)$$

In Equation 11b, σ_0 is a function of z_{max}, and B_1 and B_2 are a function of $(L - z_{max})$ while in Equation 11c, B_1 and B_2 are a function of the full debond length, L.

It should be noted that in reality the stability for fibre debonding is impaired significantly by the testing conditions (e.g. soft testing machine, long free fibre length, etc.) so that debonding could become unstable even for $L > z_{max}$ and in composites with $z_{max} \approx 0$. In fact, the experimental value $z_{max} = 15$ mm, above which stable debonding is observed, for release agent coated steel wire–epoxy composites (Fig. 2) is greater than the predicted values of either 6.5 or 5.8 mm based on Hsueh's theory or the simplified solution given in Equation 10 by a factor of about two. Moreover, when the embedded fibre length, L, is very short, the precipitous load drop after complete debonding may be aggravated by the release of the strain energy stored in the stretched fibre. The load drops to zero if the fibre is completely pulled out from the matrix. Alternatively, if the fibre is regripped by the clamping pressure exerted by the surrounding matrix material frictional pull-out of the fibre recurs.

The maximum embedded fibre length, L_{max}, above which the fibre breaks without being debonded and pulled out for a given composite system can be evaluated by equating the solution for the maximum debond stress, σ_d^*, to the fibre tensile strength, σ_t (which is measured on a gauge length identical to the free fibre length used in fibre pull-out tests). Gao *et al.*'s model gives

$$L_{max} = (1/\lambda) \ln [(\bar{\sigma} - \sigma_0)/(\bar{\sigma} - \sigma_t)] \quad (12a)$$

For a similar treatment in Hsueh's model, z_{max} value needs to be determined beforehand. If the simplified solution [24] is used

$$L_{max} = a(\sigma_t - \sigma_0)/2\tau_f + z_{max} \quad (12b)$$

In Equation 12b, σ_0 is the frictionless debond stress determined at $z = z_{max}$. It is noted that the L_{max} values (= 800 μm, 49.3 mm and 23.3 mm for the carbon fibre–epoxy matrix and untreated and acid-treated SiC fibres–glass matrix composites, respectively) estimated by using Gao *et al.*'s model in Equation 12a are comparable to those ($L_{max} = 914$ μm, 51.0 and 25.0 mm) obtained from the numerical treatment of Hsueh's model. These predictions are approximately the same as the experimental L_{max} values (51.0 and 21.7 mm) for the untreated and acid-treated SiC fibres–glass matrix composites. For the carbon fibre–epoxy matrix composite, up to $L = 420$ μm has been tested without fibre breakage (i.e. the experimental L_{max} value should be greater than 420 μm for this composite). However, the simplified solution in Equation 12b which is based on a constant τ_f value predicts significantly smaller L_{max} values (= 300 μm, 25.9 and 14.4 mm), by almost a factor of two, due to the overestimate of the friction stress component which results in unnecessarily large maximum debond stress, σ_d^*, as mentioned earlier. A similar comparison may not be worthwhile for the steel wire–epoxy matrix composites because the steel wire exhibits nonlinear plastic deformation near the breaking stress which makes the estimation of L_{max} values rather inaccurate.

3.4. Comparison of maximum debond stress, σ_d^*, and frictional pull-out stress, σ_f, between theories and experiments

The maximum debond stress, σ_d^*, and the initial frictional pull-out stress, σ_f, calculated based on the two theories (i.e. Equations 9 and 3 for Gao *et al.*'s model and Equations 11a–c and 7 for Hsueh's model) are compared with experimental results for different composites as shown in Figs 5–7. Although slight improvement in the interfacial bond strength were observed for some electrolytically oxidized carbon fibres, for simplicity they are treated in the same data

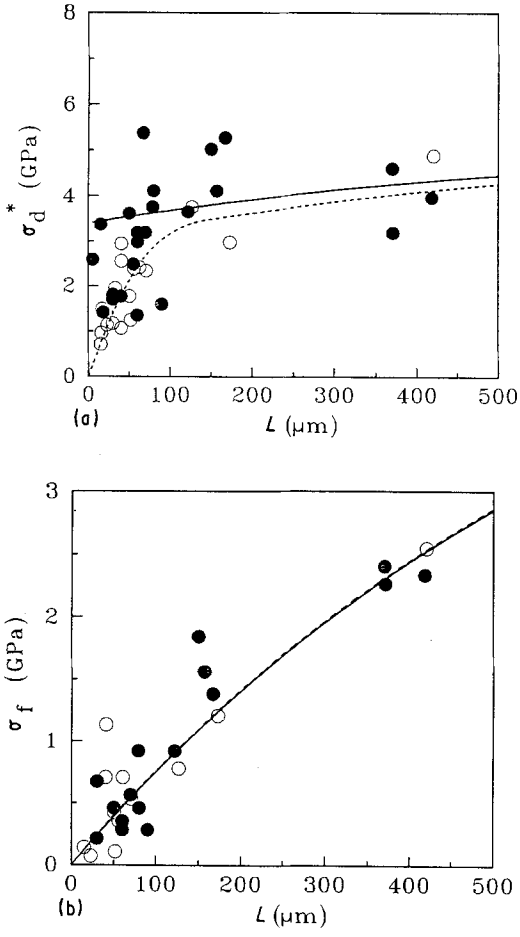

Figure 5 Comparison of experimental results and theoretical predictions of (a) maximum debond stress, σ_d^*, and (b) initial frictional pull-out stress, σ_f, as a function of embedded fibre length, L, for carbon fibre–epoxy matrix composites. Experiments: (○) untreated fibres; (●) oxidized fibres. Theories: (——) Gao *et al.* [17]; (– – –) Hsueh [12].

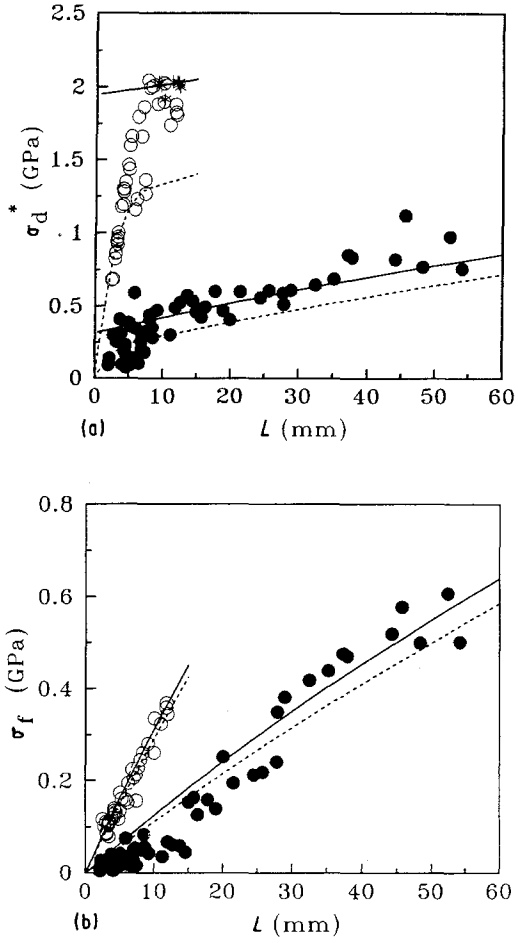

Figure 6 Comparison of experimental results and theoretical predictions of (a) maximum debond stress, σ_d^*, and (b) initial frictional pull-out stress, σ_f as a function of embedded fibre length, L, for stainless steel wire–epoxy matrix composites. Experiments: (○) uncoated wires; (●) release-agent coated wires; (×) broken wires without being pulled out. Theories: (——) Gao *et al.* [17]; (– – –) Hsueh [12].

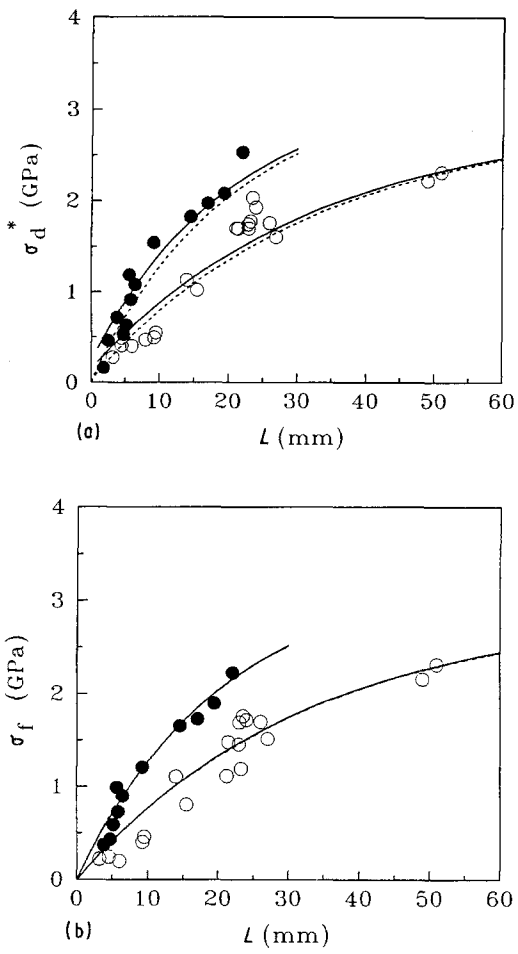

Figure 7 Comparison of experimental results and theoretical predictions of (a) maximum debond stress, σ_d^*, and (b) initial frictional pull-out stress, σ_f, as a function of embedded fibre length, L, for SiC fibre–borosilicate glass matrix composites. Experiments: (○) untreated fibres; (●) acid treated fibres. Theories: (——) Gao *et al.* [17]; (– – –) Hsueh [12].

group as the untreated fibres with identical interfacial properties in Fig. 5.

Varying degree of agreement is obtained for σ_d^* between both theories and experiments depending on the composite systems used and embedded fibre lengths (Figs 5a, 6a and 7a). For the two epoxy-based matrix composite systems (Figs 5a and 6a), Gao *et al.*'s model predicts the trend of σ_d^* well for long L, but it always overestimates σ_d^* for very short L (i.e. $L < z_{max}$). This raises several problems on the validity of the assumptions made in Gao *et al.*'s model which include: a constant G_{ic} (or σ_0) value for debonding, stable debond propagation for all embedded fibre length, L, and more importantly, the strain energy stored in the bonded region which is neglected in the analysis. In contrast, although Hsueh's model has a capability to describe the details of σ_d^* for very short L (i.e. $L < z_{max}$), it tends to underestimate slightly σ_d^* as L is increased. Therefore, in using Hsueh's model significant adjustment to the pull-out parameters (particularly the bond shear strength, τ_b, or the frictionless debond stress, σ_0) is necessary if the predicted curves are to fit the experimental results for long L. For example, provided that the values for other parameters λ and $\bar{\sigma}$ are correctly determined and thus are kept the same, a better agreement of Hsueh's model with experimental results for steel wire–epoxy matrix composites (Fig. 6a) for long L requires τ_b to be increased from measured values of 43.5 MPa to approximately 65 MPa (which is rather impractical because this value is close to the tensile strength of the epoxy matrix 66.5 MPa) and 9.0 MPa to approximately 15 MPa for the uncoated and release-agent coated wires, respectively. A similar conclusion may be drawn for the carbon fibre–epoxy matrix composite (Fig. 5a) where the measured τ_b value (72.7 MPa, which is already greater than the tensile strength of the epoxy matrix) needs to be further increased for better fit of the experimental data. In contrast to the results for other two epoxy-based matrix composite systems, for the ceramic-based matrix composite system (Fig. 7a), σ_d^* curves predicted by both theories agree exceptionally well with experiments over almost the whole range of L. This is because G_{ic} or σ_0 are so small that the two models give similar predictions.

With respect to the initial frictional pull-out stress, σ_f, there is very good agreement between theories and experiments for all the composite systems used (Figs 5b, 6b and 7b). Clearly, the predicted σ_f from the two theories agree well with each other, particularly

for the carbon fibre–epoxy matrix (Fig. 5b) and SiC fibre–glass matrix composite systems (Fig. 7b). This suggests that the solutions for σ_f proposed in the two different models are physically the same for fibre pull-out after complete debonding. In fact, such a suggestion has been proven by comparing the pull-out parameters used in the two models. It was found for all the composite systems used that the calculated value m_2 (positive) was at least two orders of magnitude greater than the value m_1 (negative) in absolute terms (i.e. $m_2 \gg m_1$). Therefore, except for very short L, the coefficients B_1 and B_2 given in Equations 6a and b (which are now a function of the entire embedded fibre length, L) can be simplified as

$$B_1 \approx (m_2 - m_1)\exp(m_1 L) \quad (13a)$$

$$B_2 \approx m_2 \quad (13b)$$

Combining Equations 13a and b with the solution for the frictional pull-out stress, σ_f, in Equation 7 in Hsueh's model, this gives

$$\sigma_f = \bar{\sigma}\left\{1 - \frac{[1 + (\gamma/\alpha)(\nu_m/\nu_f)](m_2 - m_1)\exp(m_1 L)}{\lambda + (\gamma/\alpha)(\nu_m/\nu_f)(m_2 - m_1)\exp(m_1 L) + m_2}\right\}$$

$$\approx \bar{\sigma}\left[1 - \frac{(m_2 - m_1)\exp(m_1 L)}{\lambda + m_2}\right] \quad b^2 \gg a^2 \quad (13c)$$

It is also noted that when $b^2 \gg a^2$ (say, the fibre volume fraction $\gamma < 10^{-3}$, as for the carbon fibre–epoxy matrix and SiC fibre–glass matrix composites), the magnitude of m_1 is very much the same as $-\lambda$ with less than 0.1% in error. Therefore, the simplified form of Equation 13c becomes exactly the same as the solution given in Equation 3 of Gao *et al.*'s model. The physical significance of the resemblance between the two models represented by the parameters $m_1 \equiv -\lambda$ is yet to be clarified, but it seems that the coefficient m_1 must be related to the shear stress transfer distance at the interface as the pull-out parameter, λ, itself indicates. The slightly underestimated σ_f values by Hsueh's theory relative to Gao *et al.*'s theory as observed in the steel wire–epoxy matrix composites (Fig. 6b) appears to be associated with the finite value of γ (= 0.0018) which cannot be neglected in Hsueh's equation. This result also suggests that the solution of Hsueh's model may be more sensitive to the fibre volume fraction, γ, than Gao *et al.*'s model.

The good agreement with experiments over the whole range of embedded fibre lengths also proves that the parameters $\bar{\sigma}$ and λ (which in turn determine the interfacial properties, q_0 and μ) evaluated based on Gao *et al.*'s model (Equations 8a, b and c) are properly chosen.

4. Discussion

As noted from the comparisons for the epoxy-based composite systems shown in Figs 5a and 6a, the maximum debond stress, σ_d^*, obtained from fibre pull-out tests diminishes toward zero as the embedded fibre length, L, is decreased to zero, which is exactly the same trend as what Hsueh's model predicts. In contrast, Gao *et al.*'s model overestimates σ_d^* values for very short L, particularly for the epoxy-based matrix composite systems, giving a constant frictionless debond stress, σ_0, for zero L. However, it should be pointed out here that single-fibre pull-out tests with very short L would not provide much practical significance because the maximum debond length which can be observed in fracture of fibre composites (whether fibres are continuous or randomly oriented unless exceptionally short fibres are used) is approximately the same order as the critical transfer length (which corresponds to half the longest embedded fibre length in pull-out tests) [16].

To predict more accurately the maximum debond stress, σ_d^*, for very short L, two modifications can be made in Gao *et al.*'s model. The first is a rising crack growth resistance behaviour (namely, the R-curve behaviour) for the interfacial fracture toughness, G_{ic}, rather than a constant value. This modification is supported by the work of Atkinson *et al.* [18]. In a study of the pull-out of glass rods from a polyurethane matrix based on the continuum mechanics approach using a finite element model along with the corresponding singularity analysis, they show that the interfacial fracture toughness, G_{ic}, increases gradually with increasing debond crack length from the surface, the maximum G_{ic} value at the full debond length reaching approximately three to five times the initial value at a small crack length depending on the method of predictions. It is also noted that the mode I component of the interfacial fracture toughness is important only at the initiation of the surface crack while the mode II component becomes dominant with debond crack propagation. The increasing G_{ic} value with debond length also requires that the debond crack must not propagate exactly along the fibre–matrix interface, but that failure occurs predominantly within the matrix material immediately surrounding the fibre (or the interphase) so that a fracture process zone of some substantial size can be developed ahead of the debond crack. This may be partly confirmed by the recent work of Cazeneuve *et al.* [26] where scanning Auger microscopy reveals a thin layer (0.6–2 nm) of epoxy matrix on the surface of pulled out carbon fibres (which otherwise could not have been detected if optical or scanning electron microscopes were used). They propose that matrix molecules are absorbed on the fibre through bonding to the surface oxygen groups during the cure cycle and that failure occurs between the first layer of these matrix molecules and the rest of the matrix. A similar conclusion has also been established from the study using scanning secondary ion mass spectroscopy [27]. With regard to the properties of the interphase compared to the bulk organic matrix material, a clear emerging view [28, 29] is that the interphase is significantly softer and is capable of very high deformation, supporting an

earlier similar hypothesis [30]. For example, Williams *et al.* [28] showed that the average modulus of the interphase of thickness about 250 μm in a single carbon fibre–epoxy matrix composites is about one-quarter of that in the bulk matrix. The effect of this soft interphase is severely mitigated by the presence of the rigid fibre which may effectively increase the modulus at the interphase very close to the fibre [28, 31]. However, details on the fracture toughness at this interphase region have not been reported. Whether the interfacial fracture toughness, G_{ic}, values increase or not, once the G_{ic}–debond length ($L - z$) relationship is known it is possible to obtain a new solution for σ_0 as a function of embedded fibre length, L. However, this requires the exact mechanisms of the R-curve to be established. Moreover, this modification cannot avoid a limitation that the R-curve still has a finite non-zero G_{ic} for debond initiation, and consequently does not exactly satisfy the requirement of zero debond stress at zero embedded fibre length.

Another modification which is more convincing than the one described above is that for very short L (i.e. $L \leqslant z_{max}$) the debond process becomes unstable [9, 10] and thus the original shear strength criterion [6–8] could control the whole fibre debond process as discussed in Section 3.3. In fact, a similar conclusion has been reported previously by other workers [32, 33]. Piggott [33] suggests that for very short L the fibre debond process in an organic matrix may be accompanied by a yielding process, an indication that shear deformation in the matrix plays an important role to determine stress distribution in the fibre for short L. To accommodate the unstable debond process in the context of fracture mechanics approach requires proper modification to the assumptions made in Gao *et al.*'s model.

The fact that Hsueh's solution tends to underestimate slightly the maximum debond stress σ_d^* as the embedded fibre length L is increased (Figs 5a and 6a) needs further discussion. It is worth recalling that the interfacial parameters λ and $\bar{\sigma}$ are determined on the basis of the experimental results for the initial frictional pull-out stress σ_f which is a function of the entire embedded fibre length, L, while the solution for the maximum debond stress, σ_d^*, in Hsueh's model is a function of the partial debond length ($L - z_{max}$). The above discrepancy appears to arise mainly from an underestimate of the frictionless debond stress σ_0 in Equation 11b due to the incorrectly defined boundary condition with associated simplifying assumptions. Therefore, Hsueh's model frequently needs an artificial increase in τ_b (and thus σ_0) for a better fit of the experimental σ_d^* data, provided λ and $\bar{\sigma}$ are correctly chosen, as mentioned in Section 3.4. In Hsueh's analysis [11] a second-order differential equation for the axial fibre stress derived from the approximate equilibrium of stresses in the fibre, matrix and interface was solved for the boundary conditions at both ends of the debonded region (Equations A16, A17 and A18 in Reference 11). Therefore, the condition for the continuity of the fibre stress distribution along the fibre direction was satisfied. Then, the partial debond stress was determined by considering the free-surface condition of the matrix (i.e. the matrix axial stress at the surface where fibre enters the matrix is zero, Equations A15 and A20 in Reference 11). All these formulations were performed for the debonded region where there was frictional resistance. However, the compatibility of the matrix axial stresses between the bonded and debonded regions was not properly accounted for. If a constant σ_0 is assumed as in [11] this condition does not cause any problem. However, if it is assumed that the instantaneous σ_0 values vary as a function of bond length z as in Reference 12, the boundary condition given by Equation A17 in Reference 11 (i.e. the fibre axial stress is equal to σ_0 at the boundary of the bonded and debonded regions) becomes invalid as the effect of matrix axial stress existing at the debonded (but frictionally connected) region is completely neglected. This would result in a discontinuity of the matrix stress distribution along the fibre direction as shown in Fig. 8 though the correct stress value at the debonded region may not be significant compared with the applied fibre stress, particularly for small fibre volume fractions (i.e. $b^2 \gg a^2$). The matrix axial stresses plotted in Fig. 8 are calculated based on Equations 6 and 8 of Reference 21 for the bonded region and Equations A10 and A15 of Reference 11 for the debonded region with assumed varying σ_0 values for the carbon fibre–epoxy matrix composite system. It is noted from Fig. 8 that the matrix stresses close to the outermost surface in the bonded region are predominantly compressive. This anomaly seems to be associated with the simplifying assumptions that stress components in the radial and circumferential directions are not considered for the stress–strain relationship in both the fibre and matrix [21]. It is expected that if the above conditions are correctly formulated in Hsueh's analysis the finite value of the matrix axial stress gives rise to the corresponding fibre stress which, in turn, increases the frictionless debond stress, σ_0, for a given bond length. This could effectively bring up the maximum debond stress, σ_d^*, close to the experimental values for long L.

In contrast to the results for the other two composite systems shown in Figs 5a and 6a that the

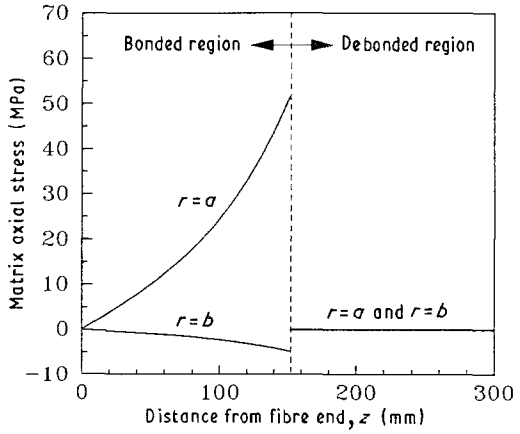

Figure 8 Plots of matrix axial stresses at the fibre–matrix interface ($r = a$) and at the outermost surface ($r = b$) along the fibre direction, z, for the carbon fibre–epoxy matrix composite with embedded fibre length $L = 300$ μm.

agreement for σ_d^* between theories and experiments is varied depending on the embedded fibre length, L, for the SiC fibre–glass matrix composites (Fig. 7a), the agreement by both models is excellent over almost the whole range of L. This appears to be a reflection of the correct assumption made in both models regarding the stability of interfacial debonding. It is worth iterating that both models originally assume stable debonding regardless of L, a condition which is actually satisfied by this ceramic composite (i.e. negligible z_{max} values both for untreated and acid-treated SiC fibres as given in Table I). If z_{max} (which is a measure of maximum embedded fibre length for unstable debond process) is compared to L_{max} (the maximum embedded fibre length which can be pulled out without fibre breakage), it is found that the SiC fibre–glass matrix composites have a ratio $z_{max}/L_{max} = 0.0008$ and 0.0036, respectively, for the untreated and acid-treated SiC fibres. For the carbon fibre–epoxy matrix composites, the ratio is approximately 0.15, and for the uncoated steel wire–epoxy matrix composites this is even larger, i.e. 0.66, if the experimental value $L_{max} = 11.9$ mm is used. Therefore, the existing solutions of the two models can be reliably used without any modification to predict both σ_d^* and σ_f if the z_{max}/L_{max} ratio is negligible.

In the comparison of the two current theoretical models, the effect of fibre radius relative to the matrix radius (or the fibre volume fraction, γ) has not been specifically examined. Certainly, one can carry out pull-out tests with different fibre radii embedded in a given matrix of constant outermost radius. This parametric study may help to evaluate whether the interfacial debonding is fracture governed or strength governed for a certain composite system [34]. In fact, Gao *et al.* [17] compared the maximum debond stress, σ_d^*, predicted by the fracture mechanics-based models of Gurney and Hunt [13], Outwater and Murphy [14] and Gao *et al.* [17] and the early shear strength-based model of Takaku and Arridge [8] with experimental data [16] on a steel wire–epoxy matrix composite systems. Gao *et al.* [17] showed that the fracture mechanics models are better and more accurately describe the debond stress than the shear strength model for a range of fibre volume fraction, γ, between 0.0001 and 0.0064 (i.e. with varying wire radii from $a = 0.1$–0.8 mm in a matrix radius $b = 10$ mm). However, this comparison for the very small range of γ does not lend any support to the conclusion that which model predicts more accurately the interfacial debonding and friction pull-out behaviour in practical fibre composites, particularly when the fibre volume fractions, γ, are as large as 0.65–0.7. In view of the fact that most debonding theories developed based on a shear lag model invariably assume a zero stress at the matrix free surface, their application to practical fibre composites may be limited to only a small γ so that any effect of interaction between fibres can be neglected. To accommodate this problem in a more rigorous analysis, it may be necessary to regard the matrix material surrounding a centrally located fibre as a circular composite the properties of which vary with γ rather than a constant value as assumed in the traditional analysis. Experimentally, pull-out specimens can be made by varying the number of fibres of a constant radius in a given matrix radius.

5. Conclusion

The present study critically examines two current theories (i.e. Hsueh [11, 12] and Gao *et al.* [17]) of fibre debonding and pull-out stresses based on the shear strength and fracture mechanics criteria, respectively. Plots of partial debond stress, σ_d^p, as a function of partial debond length $(L - z)$ identify three different cases of interfacial debond process using the instability condition $(d\sigma_d^p/dz \leqslant 0)$: (i) totally unstable for $L \leqslant z_{max}$; (ii) partially stable for $L > z_{max}$; (iii) totally stable when $z_{max} \approx 0$, where z_{max} is the maximum bond length below which the debond process becomes unstable. The stability is governed not only by elastic constants, relative volume of the fibre and matrix but more importantly by the nature of bonding at the interface and embedded fibre length. For each debond process, solutions for the maximum debond stress, σ_d^*, in Hsueh's model are given.

Comparisons of the maximum debond stress σ_d^* between the two theories and experimental results of epoxy-based matrix composite systems show that Gao *et al.*'s model predicts the trend of σ_d^* very well for long L but it always overestimates σ_d^* for very short L. In contrast, Hsueh's model has the capability to predict σ_d^* for short L, but it frequently needs significant adjustment to the parameter τ_b for a better fit of the experimental data for long L. For a ceramic-based matrix composite, σ_d^* predicted by the two models agree exceptionally well with the experiment over almost the whole range of L, a reflection that the stable debond process assumed in these theories is achieved in practice because $z_{max} \approx 0$.

With respect to the initial frictional pull-out stress, σ_f, after complete debonding, the agreement between the two theories and experiments is excellent for all L and all composite systems. Comparison of the calculated values for the pull-out parameters reveals that the solutions for σ_f proposed by the two models are essentially identical if the fibre volume fraction, γ, is negligible. This means that Gao *et al.*'s model can be more conveniently used than Hsueh's model to determine accurately the important interfacial properties such as residual clamping stress, q_0, and coefficient of friction, μ.

It is quite obvious that Gao *et al.*'s model needs some modification if an accurate prediction of σ_d^* is sought for very short L. These include varying interfacial fracture toughness, G_{ic}, with debond crack growth, unstable debonding for very short L, and inclusion of shear deformation in the matrix for the evaluation of G_{ic} and fibre stress distribution. Further work is required to obtain refined solutions of Gao *et al.*'s model in the context of a fracture mechanics approach. The details of this will be reported in Part 2 [35]. Hsueh's model may also be improved to obtain a better solution for the fibre stress during progressive debonding by including the effect of matrix axial stress existing at the debonded region.

Acknowledgements

The authors thank the Australian Research Council for continuing support of this work which forms part of a larger project on "Development of High Strength and High Fracture Toughness Composites with Controlled Interfaces". They also thank B. Cotterell and M. V. Swain for many useful suggestions and stimulating discussions. The use of facilities at the United Kingdom Royal Aerospace Establishment is also acknowledged where the pull-out tests of carbon fibre–epoxy matrix composites were carried out. One of us (JKK) is supported by an Australian Postgraduate Research Award, a P. N. Russell Scholarship and a Junior Research Fellowship.

References

1. J. K. KIM and Y. W. MAI, *Comp. Sci. Tech.* **41** (1991) 333.
2. A. KELLY and W. R. TYSON, *J. Mech. Phys. Solids* **13** (1965) 329.
3. A. KELLY, *Proc. R. Soc. Lond.* **A282** (1964) 63.
4. B. MILLER, P. MURI and L. REBENFELD, *Comp. Sci. Tech.* **28** (1987) 17.
5. M. K. TSE, *SAMPE J.* **21** (1985) 11.
6. H. L. COX, *Brit. J. Appl. Phys.* **3** (1952) 72.
7. L. B. GRESZCZUK, "Interfaces in Composites", ASTM STP 452 (American Society for Testing and Materials, Philadelphia, 1969) p. 42.
8. A. TAKAKU and R. G. C. ARRIDGE, *J. Phys. D Appl. Phys.* **6** (1973) 2038.
9. P. LAWRENCE, *J. Mater. Sci.* **7** (1972) 1.
10. V. LAWS, P. LAWRENCE and R. W. NURSE, *J. Phys. D Appl. Phys.* **6** (1973) 523.
11. C. H. HSUEH, *Mater. Sci. Engng* **A123** (1990) 1.
12. *Idem, ibid.* **A125** (1990) 67.
13. C. GURNEY and J. HUNT, *Proc. R. Soc. Lond. A* **299** (1967) 508.
14. J. O. OUTWATER and M. C. MURPHY, in "Proceedings of the 24th Conference on SPI" (1969) Paper 11C.
15. H. STANG and S. P. SHAH, *J. Mater. Sci.* **21** (1986) 953.
16. J. K. WELLS and P. W. R. BEAUMONT, *ibid.* **20** (1985) 1275.
17. Y. C. GAO, Y. W. MAI and B. COTTERELL, *J. Appl. Math. Phys. (ZAMP)* **39** (1988) 550.
18. C. ATKINSON, J. AVILA, E. BETZ and R. E. SMELSER, *J. Mech. Phys. Solids* **30** (1982) 97.
19. C. K. Y. LEUNG and V. C. LI, *Composites* **21** (1990) 305.
20. *Idem, J. Mater. Sci.* (1992) in press.
21. C. H. HSUEH, *J. Mater Sci. Lett.* **7** (1988) 497.
22. E. P. BUTTLER, E. R. FULLER Jr and H. M. CHAN, *Mater. Res. Soc. Symp. Proc.* **170** (1990) 17.
23. J. K. KIM, C. BAILLIE and Y. W. MAI, *Scripta Metall. Mater.* **25** (1991) 315.
24. V. M. KARBHARI and D. J. WILKINS, *ibid.* **24** (1990) 1197.
25. J. D. BRIGHT, S. DANCHAIVIJIT and D. K. SHETTY, *J. Amer. Ceram. Soc.* **74** (1991) 115.
26. C. CAZENEUVE, J. E. CASTLE and J. F. WATTS, *J. Mater. Sci.* **25** (1990) 1902.
27. P. DENISON and F. R. JONES, *ibid.* **23** (1988) 2153.
28. J. G. WILLIAMS, M. E. DONNELLAN, M. R. JAMES and W. L. MORRIS, *Mater. Sci. Engng* **A126** (1990) 305.
29. T. C. TSAI, A. M. AROCHO and L. M. GAUSE, *ibid.* **A126** (1990) 294.
30. M. R. PIGGOTT, *Polym. Comp.* **8** (1987) 291.
31. G. C. PAPANICOLAOU, G. J. MESSINIS and S. S. KARAKATSANIDIS, *J. Mater. Sci.* **24** (1989) 395.
32. P. BARTOS, *ibid.* **15** (1980) 3122.
33. M. R. PIGGOTT, *Comp. Sci. Tech.* **30** (1987) 295.
34. C. K. Y. LEUNG and V. C. LI, *J. Mater. Sci. Lett.* **9** (1991) 1140.
35. L-M. ZHOU, J-K KIM and Y-W MAI, *J. Mater. Sci.* (1992) **27**, 3155.

Received 7 January
and accepted 13 May 1991